Highly Concentrated, Intercalated Silicate Nanocomposites: Synthesis and Characterization

Adam S. Zerda, Terrence C. Caskey, and Alan J. Lesser*

Polymer Science and Engineering, University of Massachusetts, Amherst, Massachusetts 01003

Received August 19, 2002

ABSTRACT: PMMA-layered silicate intercalated nanocomposites are synthesized using supercritical carbon dioxide ($scCO_2$) to produce ordered materials with significant levels of reinforcement. The $scCO_2$ is used to homogeneously distribute monomer as well as act as a low-viscosity solvent for MMA polymerization. This route allows for synthesis of nanocomposites containing significant levels of organically modified layered silicates (OMLS). Below 40 wt % OMLS, the intercalated nanocomposites exhibit a *d* spacing commensurate with dimensions of the fully extended surfactant chains. Above 40 wt % OMLS, the composite volume is saturated with inorganic material, and the *d* spacing decreases to homogeneously distribute the polymer volume. A model for estimating this transition concentration is presented. At concentrations approaching the homogeneously intercalated morphology, the basic mechanical and physical properties of the composite are investigated.

Introduction

Recently, a great deal of attention has been focused on developing and characterizing materials that incorporate nanosilicate reinforcements. To this end, significant strides have been made to incorporate these types of reinforcement into a variety of polymeric materials.[1−12] Interest in these materials stems from the fact that, in many cases, interesting physical and mechanical properties have been reported. Consequently, there has been a great deal of discussion regarding the unique physical state of the polymer at the silicate−polymer interface and its associated effect on the mechanical properties of the composite.[13] However, there are also other aspects related to the mechanical toughness that arise from the unique combination of both nanosilicate size together with its highly anisotropic shape (i.e., high aspect ratio) that warrant further investigation.

In general, two idealized morphologies can be developed using the nanosilicate fillers: intercalated (platelets retain proximity and order) and exfoliated (platelets are delaminated and disbursed). Exfoliated clay nanocomposites can be synthesized through a number of different routes, including in-situ polymerization,[5,6] melt intercalation,[8] and silicate crystallization from polymer−silicate gel precursors.[2,14] The stiffness is always shown to increase with this morphology, but the toughness is shown to diminish in many glassy systems when tested below their glass transition (T_g). Many systems do not achieve a fully exfoliated structure and also contain a partially delaminated intercalated phase.

The intercalated morphology consists of well-ordered alternating layers of polymer and silicate. The *d* spacing of these hybrids is easily recognized using wide-angle X-ray diffraction (WAXD), with typically a few nanometers separating individual platelets in a lamellar-like stacked morphology. Morphologically, intercalated nanocomposites are capable of property enhancements unavailable to the exfoliated systems. The combination of the spatial configuration produced in the intercalated phase, the modulus mismatch between the polymer and silicate, and the high aspect ratio of the silicates produces high stress concentrations at the silicate edges that mechanically interact with other silicates within their certain proximity. Enabling the individual silicates to interact allows for cooperative mechanisms of energy dissipation to occur in the polymer over much larger length scales relative to the individual silicates, thereby enhancing the fracture toughness.[15] To study this phenomenon, it is first necessary to synthesize intercalated nanocomposites with high clay content.

Incorporation of high concentrations of nanometer-scale silicates into a composite is problematic due to both the size and aspect ratio of the silicates. Hydrodynamic analysis of fluids containing rigid particles with high aspect ratios shows that the viscosity of the medium is greatly increased in a commensurate fashion as the elastic modulus of the glass is altered by the rigid reinforcement. Moreover, the viscosity of a solid−liquid mixture is affected by the interaction surface area between the two components. Nanoscale fillers have, by virtue of their small dimensions, large surface areas. Montmorillonite, for example, possesses 700 m^2/g of accessible surface area.[16] At concentrations above 20 wt % modified silicate, the viscosity of a monomer−silicate mixture becomes such that homogeneous dispersion is arduous and defect formation is common.

In this paper, we present a synthetic route to produce polymer-based nanosilicate composites that have high silicate concentrations and are highly ordered. The challenges of high viscosity apparent at silicate concentrations above 20 wt % are overcome by using supercritical CO_2 ($scCO_2$) as a reaction medium. Homogeneous dispersion of monomer, initiation, and subsequent polymerization all occur under a lower viscosity in this medium. Previous applications of supercritical CO_2 as a plasticization medium, where the polymer is not soluble, include enhanced fiber drawability,[17,18] solvent welding,[21] and phase-selective modification of multiphase systems.[20−23] Depressurization upon completion of the polymerization results in reversible extraction of the CO_2 gas in a manner significantly superior to traditional solution techniques. This route can also be used to synthesize nematic architectures where the platelets exhibit preferential order.

10.1021/ma0213450 CCC: $25.00
Published on Web 02/11/2003

Table 1. Montmorillonite Clays: Physical Data

clay	*d* spacing (Å)	surface modification[a]	surface charge (meg/100 g)
Na-mont	10.7	none	N/A
C15A	30.6	2M2HT	125
C20A	24.2	2M2HT	95
C25A	18.6	2MHTC8	95

[a] HT = hydrogenated tallow (65% C 18, 30%, C 16, 5%, C 14), 2M = dimethyl, C8 = 2-ethylhexyl.

Experimental Section

Materials. To incorporate monomer into the gallery spacing, the aluminosilicates must be modified to yield an increased *d* spacing and to provide an organophilic surface for the monomer. The modified clays used in this study are montmorillonite-based silicates obtained from Southern Clay Products. The following discussion focuses on three specific organically modified layered silicates (OMLS), each with a different initial *d* spacing (Table 1). Cloisite 15A and 20A are each modified with a dialkyldimethylammonium salt from hydrogenated tallow. The difference in *d* spacing is due to the difference in the surface charge density of the base silicate. C15A has a larger charge density and therefore results in a more tightly packed surfactant layer upon modification. Cloisite 25A is modified with an asymmetric dialkyldimethylammonium surfactant and exhibits a smaller initial *d* spacing than either C15A or C20A. The matrix polymer for the synthesized nanocomposites is poly(methyl methacrylate), PMMA, radically polymerized in supercritical CO_2. To synthesize high-molecular-weight polymer efficiently, the methyl methacrylate (MMA) monomer is distilled to remove inhibitors. The radical initiator is *tert*-butyl peroxybenzoate (TBPB), which has an activation temperature of approximately 100 °C. The half-life of the initiator is considered infinite at 65 °C. Both monomer and initiator were obtained from Sigma-Aldrich.

Apparatus. Composites are fabricated in a custom-made high-pressure apparatus (Figure 1) specifically designed to allow for the application of a compressive normal force to the samples while in the presence of $scCO_2$. The normal force allows for controlled volume changes during polymerization and allows for orientation to be simultaneously imposed during the process. The details of this experimental apparatus have been discussed elsewhere,[19] but the main points of the system are reiterated here. The reaction vessel is a stainless steel cavity, 10 cm in diameter, which is mounted in a hydraulic press. The CO_2 pressure is controlled via an electronic pressure regulator with a computer interface that allows for fine pressure control. Thermocouples penetrate the body of the vessel and allow for accurate monitoring and control of temperature. The CO_2 pressure can be dynamically controlled via an ER 3000 pressure regulator or by virtue of a backpressure regulator. The latter allows for controlled $scCO_2$ flow through the reaction chamber and can be used to remove excess monomer. A monomer reserve is also incorporated into the design to allow for a true reaction-injection molding (RIM) synthetic route.

Composite Synthesis. The silicate nanocomposites are synthesized by adding a known amount of OMLS, MMA monomer, and initiator into the reaction vessel. Note that mixing is not required. The vessel is then closed and placed in the press with approximately 5 MPa of compressive normal pressure acting on the top of the chamber. The mold is then pressurized to between 10 and 14 MPa with CO_2 at room temperature, and the main valve is closed. The chamber is then allowed to equilibrate at 65 °C for 4 h, at which point the temperature is increased to 110 °C for an additional 6 h. The initial 65 °C stage is termed the soak stage while polymerization occurs at 110 °C. After reaction, the temperature is allowed to drop and the mold valve is returned to dynamic pressure control from the ER 3000. The pressure is then dropped slowly to ambient conditions over a 15 h period.

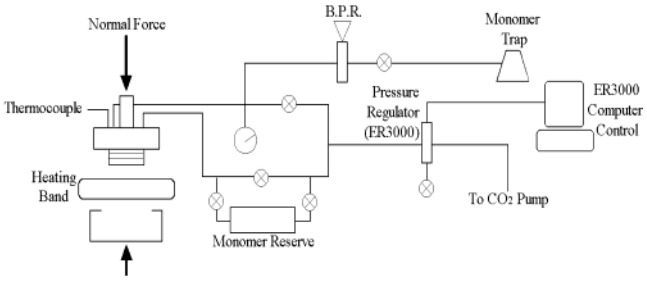

Figure 1. Schematic of supercritical CO_2 reaction vessel.

This final stage of composite synthesis is referred to as the consolidation stage as normal force can again be applied to the top of the chamber, compacting the sample and inducing a nematic orientation to the silicates. Following synthesis, residual CO_2 trapped within the polymer must be removed.[24] This is done alternatively by evacuation of the composite at 50 °C for a period of days or through melt-processing of the sample. The composite is heated above T_g and deliberately foamed, thereby removing all CO_2. The foam is pulverized and melt-pressed into a plaque.

Characterization. The composites are characterized in terms of their nanoscale morphology using a combination of scanning electron microscopy (SEM) and small-angle X-ray scattering (SAXS). SEM images were obtained on a JEOL FE-SEM microscope using a 5 kV accelerating voltage to minimize damage to the PMMA surface. SAXS patterns were obtained on a Rigaku RU-200 rotating anode diffractometer with Fuji AS-Va image plates.

In addition to the morphological characterization, the samples were studied for the effect of the high clay concentrations on thermal and mechanical properties. The thermal properties of the cured resins were investigated using both differential scanning calorimetry (DSC) and dynamic mechanical thermal analysis (DMTA). The scanning rate was 10 °C/min for DSC and 5 °C/min for DMTA at 1 Hz while imposing a 0.05% dynamic strain. Thermal degradation measurements were made employing thermogravimetric analysis (TGA) on a TA 2050 at a heating rate of 40 °C/min from room temperature to 800 °C. Samples were run under a nitrogen purge, although no significant differences were apparent in char yield and degradation rate when degradation occurs in air. Mechanical measurements of modulus were obtained from the DMTA as well as in tension according to ASTM D638. Tensile samples were loaded at a strain rate of 0.15 s^{-1}, using extensometers for strain measurements. Molecular weight measurements of the polymer were carried out in THF. The composites were dissolved under moderate sonication to free intercalated polymer. A PMMA synthesized under identical conditions in $scCO_2$ without silicate was used as a control. All of the PMMA synthesized was of high molecular weights (>200 000 g/mol).

Results and Discussion

Morphology. Nanocomposites potentially garner their material improvements from interactions on the molecular scale, influencing physical and material parameters at scales inaccessible by traditional filler materials. However, from length scale arguments it is also known that toughening occurs over a specific size range, and effective toughening may not be energetically favorable at nanolength scales. Toughening generally necessitates a particulate size greater than 0.1 μm if a cavitation or particle debonding type of mechanism is to be realized.[25] This size effect arises from the fact that exfoliated particles are too far apart to interact effectively, and the energy associated with cavitation or debonding is a function of the strain energy in the particle (which, in turn, is a function of the particle

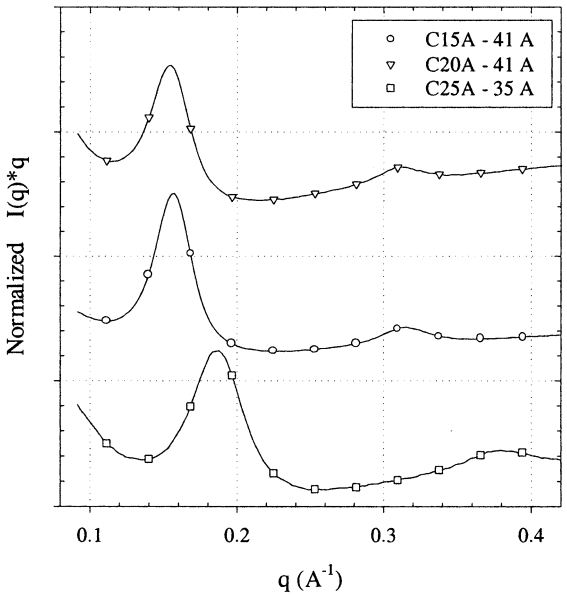

Figure 2. Intercalated clays in PMMA matrix. Samples all contain approximately 20 wt % OMLS. Data are continuous; open points are for identification only.

volume) while the energy barrier for this process is associated with the surface area of the particle or the cavitated region. Thus, below a critical size, the available energy for this process cannot overcome the associated barrier, and therefore no mechanisms of energy dissipation become operative in the material. Similar scale limitations exist for other mechanisms as well. For example, the nanoparticles are generally too small to provide toughening through a crack-bridging mechanism, and they cannot effectively enhance crack trajectory tortuosity. Therefore, the extremely reduced scale of a fully exfoliated nanocomposite does not lend itself to applications where energy is absorbed, as is the case for materials below their T_g.

In contrast, the intercalated morphology allows polymer into the galleries between silicates but does not fully delaminate them into the completely exfoliated structure. Since the silicates have a high aspect ratio and exhibit a high modulus mismatch (between silicate and polymer), they can interact with other silicates within their proximity. The nature of this interaction can be either shielding or amplification and is intimately associated with the relative configurational positions of the silicates while the strength of the interaction is associated with the tip-to-tip distance between silicates. However, before these interactions can be investigated systematically, materials containing higher concentrations of the intercalated structure must be fabricated with controlled spacings between nanosilicates.

Intercalated nanocomposites of constant clay concentration (20 wt % OMLS) were synthesized using silicates of differing surface modification in order to determine the effect of the modifier in dictating the maximum clay concentration and degree of intercalation. SAXS was conducted on each composite, and the results are shown in Figure 2. The *d* spacing of the nanocomposites based on the C15A and C20A, which vary in initial gallery spacing due to the difference in clay charge density, are equal because each is modified by the same alkylammonium surfactant. The length of the surfactant, not the clay charge density, dictates the final intercalated separation here. The third composite (based on C25A)

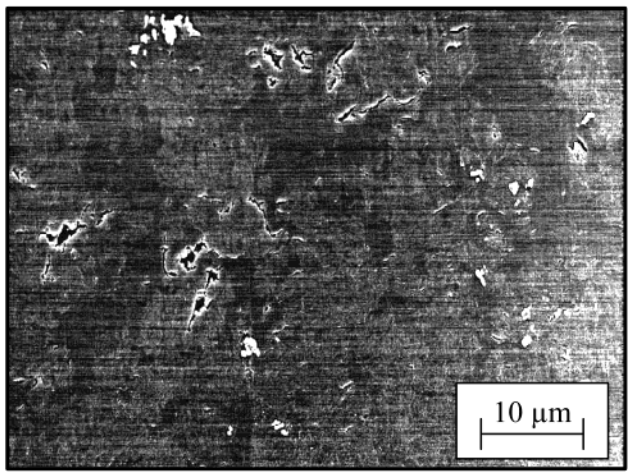

Figure 3. SEM micrograph of 20 wt % OMLS in PMMA. At this clay concentration, half of the available volume in the sample is consumed by the silicate-rich intercalated morphology.

results in a small intercalated *d* spacing due to its shorter surfactant length. At these low clay concentrations (~20 wt %) the microscale morphology is heterogeneous with distinct regions rich in clay surrounded by a polymer-rich matrix (see Figure 3).

It is interesting to note that at low clay concentrations the *d* spacing of the intercalated nanocomposite is constant, regardless of the amount of polymer introduced. This results in a maximum intercalated separation and is a consequence of the thermodynamics of intercalation. Intercalation is an enthalpically driven process which is limited by the entropic penalty for polymer confinement.[26] The enthalpic contributions during intercalation are sufficient to induce wetting of the intragallery regions of the OMLS. Initially, the galleries between silicates are swollen, and the decrease in entropy of intercalated monomer or polymer is countered by the degrees of freedom gained during surfactant swelling. The free energy of the system is then decreased. Once these surfactants have reached a maximum extension, further intercalation increases the free energy, and the maximum intercalated *d* spacing is maintained regardless of concentration. The *d* spacing of the intercalated morphology is, therefore, strongly dictated by the architecture of the silicate modifiers.

Additional composites were synthesized with higher clay concentrations in order to evaluate the limits of this synthetic method and assess its effect on the overall morphology. Figure 4 shows the effect that nanosilicate concentration has on the *d* spacing between galleries. Note that below a concentration of 30 wt % the *d* spacing remains unchanged, but at 50 wt % the *d* spacing decreases and the scattering peak is broader and not as well-defined. This suggests that 50 wt % may be above a critical concentration where the composite is starved for polymer.

To assess whether the 50 wt % composite is indeed above a critical concentration, an estimate of the critical concentration is necessary. Consider a polymer−clay ratio, *f*, that results in a saturation of the modified clay surface upon blending. This concentration can be estimated by taking the product of the polymer density, ρ_p, surface area of the silicate, S_{OMLS}, in m^2/g, and the polymer contribution to the composite gallery spacing. This latter property is estimated as the difference between the gallery height of the intercalated nano-

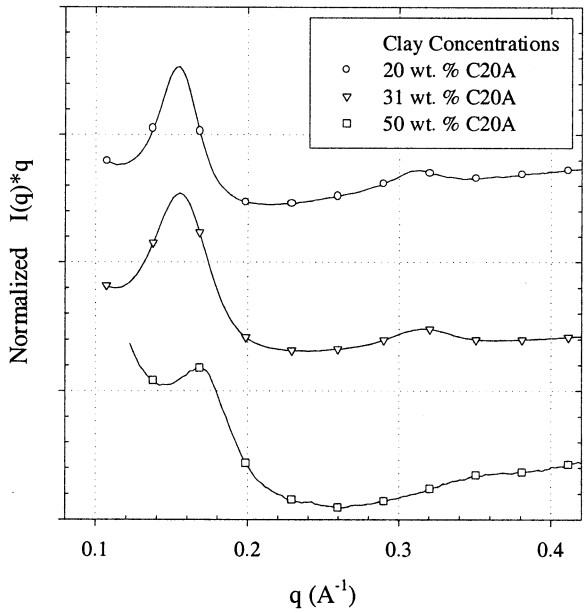

Figure 4. Effect of increased clay concentration on lamellar ordering and *d* spacing of intercalated nanocomposite. Data are continuous; open points are for identification only.

composite, d_c, and the initial *d* spacing of the OMLS, d_{OMLS}. This is shown in the following equation:

$$f = \frac{m_p}{m_{OMLS}} = \rho_p(d_c - d_{OMLS})S_{OMLS} \qquad (1)$$

In eq 1, a number of assumptions are made. First, the increase in the gallery height upon composite formation is attributed solely to incorporation of polymer between silicate stacks. Mixing of polymer with the surfactant chains occurs with no significant change in the total free volume. Second, the density of the polymer within the gallery is assumed to equal the bulk density of the polymer.[27,28]

Equation 1 predicts that the maximum ratio for the case of the C20A−PMMA nanocomposite ($\rho_p = 1.2$ g/cm^3, $S_{OMLS} = 700$ m^2/g, change in *d* spacing = 18 Å) is approximately 1.45:1, or 40 wt % OMLS. Below 40 wt % OMLS, the *d* spacing does not change with the amount of clay in the composite (Figure 4). This is in keeping with what is shown for intercalated systems. Above 40 wt % OMLS, however, the *d* spacing is decreased as there is not enough polymer available to further swell the clay. Rather than form a two-phase material containing regions of both fully intercalated and completely unswollen clay, the polymer is distributed evenly throughout, resulting in a smaller average intercalated *d* spacing. There is no evidence of a peak at 24.2 Å ($q = 0.26$ Å^{-1}) corresponding to the unswollen C20A clay. This result indicates that the $scCO_2$ method does provide homogeneous dispersion of the monomer throughout the volume prior to polymerization.

Equation 1 can also be used to estimate the response of an intercalated nanocomposite containing a clay concentration greater than the above estimated value. At these higher clay concentrations, the nanocomposite is starved for polymer and fully swollen gallery spacing is not achievable. The peak corresponding to the 50 wt % clay sample is broader and less defined than those for the lower clay concentrations. This indicates a broader distribution of gallery spacings within the composite. The *d* spacing has also decreased to 36.9 Å ($q = 0.17$ Å^{-1}). This value is close to that estimated by eq 1 (35.9 Å).

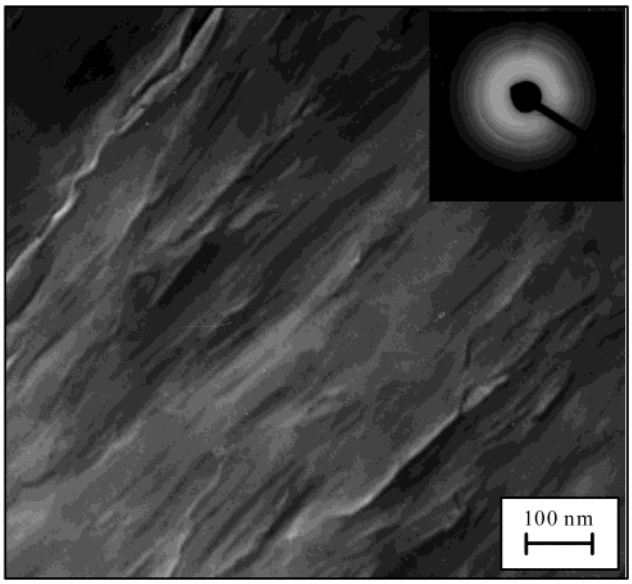

Figure 5. TEM micrograph of a 40 wt % clay nanocomposite in PS matrix. The inset electron diffraction pattern exhibits the characteristic isotropic lamellar ring.

To verify a homogeneously intercalated morphology devoid of clay-rich and polymer-rich phases, TEM images of a 40 wt % clay sample were obtained (Figure 5). To obtain such images, the matrix material was changed from PMMA, which ablates readily in the electron microscope, to polystyrene (PS). The image is representative of the entire sample volume, indicating a homogeneously intercalated gross morphology. Regions devoid of the intercalated structure are not observed as is the case for the lower silicate concentrations.

Nematically oriented nanocomposites can also be synthesized. This orientation is achieved in one of two ways. The first takes advantage of the reaction vessel design. As the chamber is depressurized, the normal force on the chamber is increased to match the drop in pressure. This consolidation decreases the volume within the vessel and induces a moderate orientation to the resulting nanocomposite. SAXS measurements of such a consolidated specimen demonstrate an orientation function $f = 0.55$ at 50 wt % clay following consolidation. The second orientation method takes advantage of the melt processability of the clay nanocomposites, which can be pressed into plaques. The melt process step induces a preferential orientation in the flow direction (Figure 6). These melt-processed nanocomposites exhibit orientation functions of $f = 0.8$ with no coherent scatter perpendicular to the orientation direction.

Physical Properties. The interest in a homogeneously intercalated morphology stems from the opportunities this system provides in terms of true polymer−ceramic hybrid properties, including enhanced mechanical properties. The mechanical performance of the intercalated nanocomposites, as well as their thermal properties, is discussed below. As many polymer material properties, including T_g, are influenced by the molecular weight of the polymer, the polymer synthesized herein was verified to be of high molecular weight (>200 000 g/mol).

The intercalated nanocomposites synthesized in this study exhibit a thermal transition near 105 °C in the

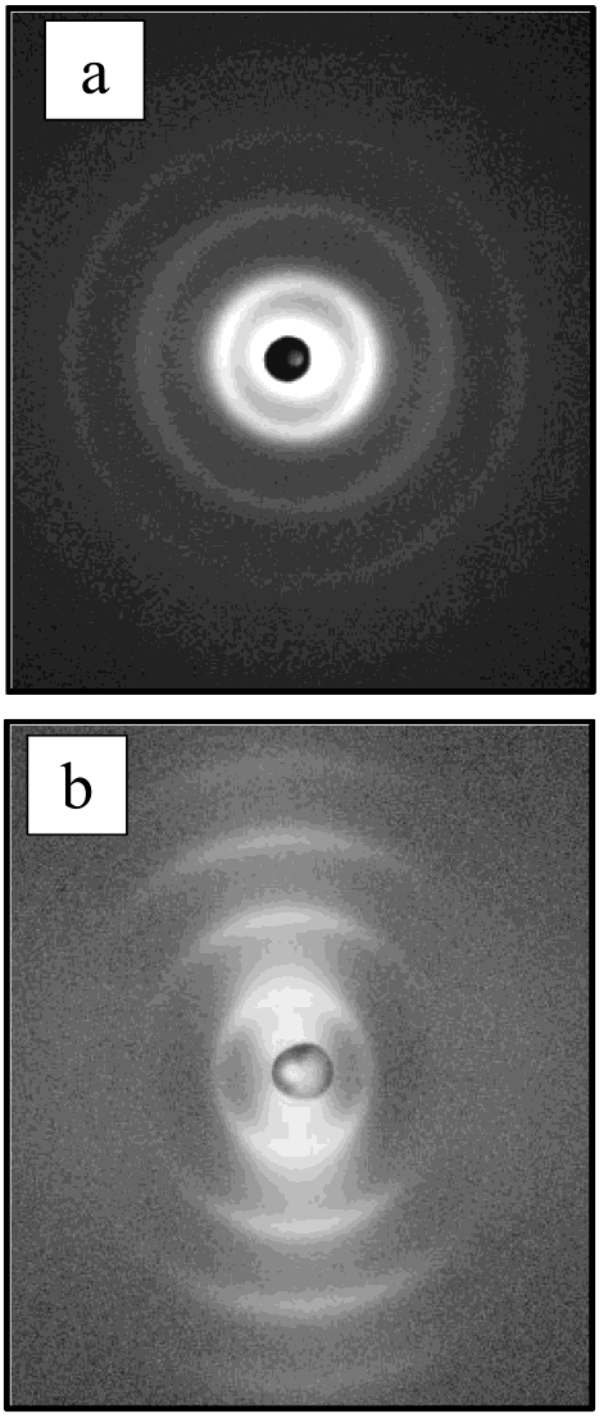

Figure 6. $scCO_2$-synthesized sample can be processed following polymerization to induce orientation, from (a) to (b). This postpolymerization processing, as with the melt-processed sample above, can induce a strongly anisotropic morphology ($f = 0.8$).

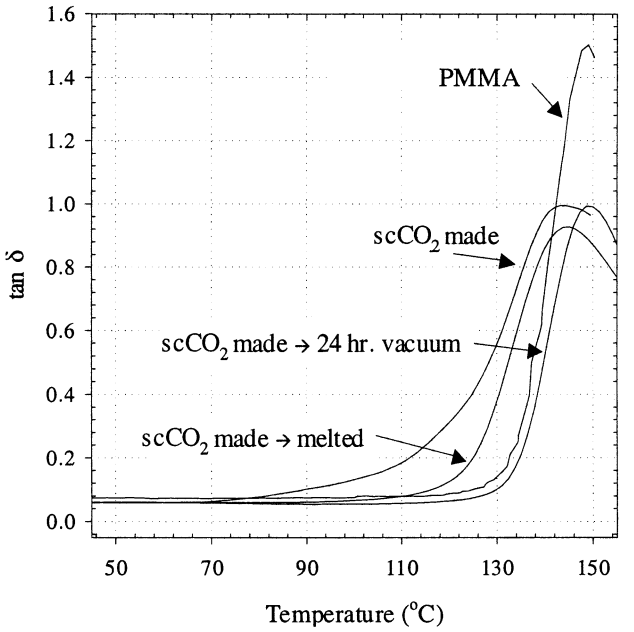

Figure 7. Loss tangent (tan δ) spectra of 40 wt % C20A nanocomposites in PMMA following various posttreatments as compared to commercial PMMA. The broad peak of the CO_2-made composite illustrates the early onset of foaming prior to CO_2 removal.

DSC, corresponding to the glass transition temperature of PMMA. At high clay concentrations, the transition is faint but reproducible, owing to the low polymer content in these composites. To analyze the thermal properties of the composite more carefully, dynamic tensile measurements under a temperature ramp were conducted in a DMTA. These are compared to a control, a commercial PMMA sample of $M_W = 1\,000\,000$ g/mol (Figure 7). All of the nanocomposites undergo a thermal transition (α-relaxation) at 150 °C according to the peak in the tan δ. This transition is similar to the α-relaxation peak of the PMMA control. This observation is significant in that it demonstrates the presence of molecular mobility of chains in a predominately intercalated structure. At 40 wt % clay, the vast majority of the polymer is confined to the intergallery spacing but continues to exhibit relaxation modes of the bulk polymer. Morphological investigations of these highly filled composites show no evidence for polymer-rich regions which would be responsible for this behavior. A second T_g is also not observed. Although the subject of mobility in confined polymers is a controversial one, these results support previous observations made by Russel et al.[29]

The tensile modulus of 40 wt % OMLS nanocomposites was determined from the storage modulus of the DMTA spectra (Figure 8). Under all conditions, the nanocomposites exhibit a significantly higher storage modulus. The "CO_2-made" curve demonstrates the need to completely remove residual CO_2 from the composites. A premature softening is observed at approximately 90 °C. This is a result of the CO_2 becoming less soluble in the polymer at higher temperatures, foaming the matrix. After the sample has been sufficiently evacuated, following 24 h in a vacuum oven at 75 °C, features relating to CO_2 plasticization are eliminated. Thus far, these materials are isotropic, but both exhibit a 50% increase in modulus. Once the composite has been oriented through melt processing, anisotropic mechanical properties are exhibited. This is observed in the CO_2-made, melt-processed sample. The curve illustrates the effectiveness of silicate orientation in achieving modulus enhancements. By inducing a nematic order to the silicates, a 220% increase in the tensile modulus is achieved for the glassy polymer. Previously, such modulus enhancements have been demonstrated only for rubbery polymers, where silicate orientation is achieved as the polymer is drawn.[3]

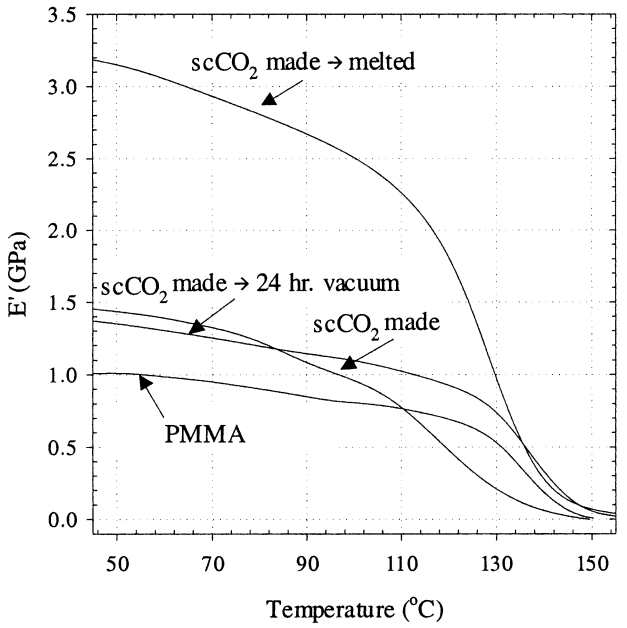

Figure 8. Storage modulus of 40 wt % C20A/PMMA composites as compared to commercial PMMA (○). The effects of CO_2 plasticization is evident when comparing the as-made sample (□) to a specimen evacuated for 24 h (◇). Postpolymerization melt processing (△), which induces orientation, results in a marked increase in modulus.

Conclusions

Intercalated nanocomposites containing modified silicates in excess of 20 wt % have been synthesized. At clay concentrations approaching 40 wt %, the silicate morphology is homogeneous, with virtually the entire polymer volume present within the gallery spacing between silicates. Because the intercalated silicate structure is thermodynamically limited with regards to clay separation, high clay concentrations are required to achieve a homogeneous morphology. A simple model of the intercalated structure is used to predict the amount of organically modified silicates required to produce such a morphology. A new synthetic route to producing intercalated nanocomposites using supercritical fluids as a reaction medium is introduced. Using $scCO_2$, the problems associated with high viscosities characteristic of highly loaded polymers are circumvented. The $scCO_2$ is used to distribute homogeneously the monomer prior to polymerization. At clay concentrations above those predicted by the model, the intercalated gallery spacing collapses linearly as the system becomes starved for polymer.

The mechanical properties of the intercalated nanocomposites demonstrate true polymer−ceramic mechanical properties. The modulus of glassy PMMA with 40 wt % OMLS is increased 50% for an isotropic composite. Orientation through melt postprocessing results in a 220% increase in the tensile modulus as measured through the DMTA. Interestingly, the fully intercalated morphology at 40 wt % clay exhibits a glass transition similar to that of bulk, unmodified PMMA.

References and Notes

(1) Lagaly, G. *Appl. Clay Sci.* **1999**, *15*, 1−9.
(2) Carrado, K. A.; Langqiu, X. *Chem. Mater.* **1998**, *10*, 1440−1445.
(3) Pinnavaia, T. J.; Lan, T. *Chem. Mater.* **1994**, *6*, 2216−2219.
(4) Giannelis, E. P.; Messersmith, P. B. *Chem. Mater.* **1994**, *6*, 1719−1725.
(5) Usuki, A.; Kojima, Y.; Kawasumi, M.; Okada, A.; Fukushima, Y.; Kurauchi, T.; Kamigaito, O. *J. Mater. Res.* **1993**, *8*, 1185−1189.
(6) Usuki, A.; Kojima, Y.; Kawasumi, M.; Okada, A.; Fukushima, Y.; Kurauchi, T.; Kamigaito, O. *J. Mater. Res.* **1993**, *8*, 1179−1184.
(7) Yano, K.; Usuki, A.; Okada, A.; Kurauchi, T.; Kamigaito, O. *J. Polym. Sci., Polym. Chem.* **1993**, *31*, 2493−2498.
(8) Giannelis, E. P.; Vaia, R. A.; Jandt, K. D.; Kramer, E. J. *Macromolecules* **1995**, *28*, 8080−8085.
(9) Pinnavaia, T. J.; Wang, Z. *Chem. Mater.* **1998**, *10*, 3769-+.
(10) Wei, K. H.; Chen, T. K.; Tien, Y. I. *Polymer* **2000**, *41*, 1345−1353.
(11) Giannelis, E. P.; Bergman, J. S.; Chen, H.; Thomas, M. G.; Coates, G. W. *Chem. Commun.* **1999**, *21*, 2179−2180.
(12) Usuki, A.; Kawasumi, M.; Hasegawa, N.; Kato, M.; Okada, A. *Macromolecules* **1997**, *30*, 6333−6338.
(13) Vaia, R. A.; Sauer, B. B.; Tse, O. K.; Giannelis, E. P. *J. Polym. Sci., Part B: Polym. Phys.* **1997**, *35*, 59−67.
(14) Carrado, K. A. *Appl. Clay Sci.* **2000**, *17*, 1−23.
(15) Zerda, A. S.; Lesser, A. J. *J. Appl. Polym. Sci.*, in press.
(16) Weaver, C. E.; Pollard, L. D. *The Chemistry of Clay Minerals*; Elsevier Scientific: New York, 1973.
(17) Hobbs, T.; Lesser, A. J. *Polym. Eng. Sci.* **2001**, *41*, 135−144.
(18) Hobbs, T.; Lesser, A. J. *J. Polym. Sci., Part B: Polym. Phys.* **1999**, *37*, 1881−1891.
(19) Caskey, T. C.; Lesser, A. J. *Polym. Eng. Sci.* **2001**, *84*, 134.
(20) Watkins, J. J.; McCarthy, T. J. *Macromolecules* **1994**, *27*, 4845−4847.
(21) Watkins, J. J.; McCarthy, T. J. *Polym. Mater. Sci. Eng. Proc. ACS Div. Polym. Mater. Sci. Eng.* **1995**, *73*, 158.
(22) Kung, E.; Lesser, A. J.; McCarthy, T. J. *Macromolecules* **1998**, *31*, 4160−4169.
(23) Vogt, B. D.; Brown, G. D.; RamachandraRao, V. S.; Watkins, J. J. *Macromolecules* **1999**, *32*, 7907−7912.
(24) Kumar, V.; Holl, M. R.; Garbini, J. L.; Murray, W. R. *J. Mater. Sci.* **1999**, *34*, 637−644.
(25) Bucknall, C. B.; Karpodinis, A.; Zhang, X. C. *J. Mater. Sci.* **1994**, *29*, 3377−3383.
(26) Vaia, R. A.; Giannelis, E. P. *Macromolecules* **1997**, *30*, 8000−8009.
(27) Wu, W.-L.; Orts, W. J.; van Zanten, J. H.; Fanconi, B. M. *J. Polym. Sci., Part B: Polym. Phys.* **1994**, *32*, 2475−2480.
(28) Fernandez, M. L.; Higgins, J. S.; Penfold, J.; Shackleton, C. S. *Polym. Commun.* **1990**, *31*, 124−127.
(29) Liu, Y.; Russell, T. P.; Samant, M. G.; Stohr, J.; Brown, H. R.; Crossy-Favre, A.; Diaz, J. *Macromolecules* **1997**, *30*, 7768−7771.

MA0213450